Title

Response inhibition is associated with white matter microstructure in children

Journal

Neuropsychologia, 48(4)

ISSN

0028-3932

Authors

Madsen, Kathrine Skak
Baaré, William FC
Vestergaard, Martin
et al.

Publication Date

2010-03-01

DOI

10.1016/j.neuropsychologia.2009.11.001

Peer reviewed

Neuropsychologia 48 (2010) 854–862

Contents lists available at ScienceDirect

Neuropsychologia

journal homepage: www.elsevier.com/locate/neuropsychologia

Response inhibition is associated with white matter microstructure in children

Kathrine Skak Madsen[a,b,c,*], William F.C. Baaré[a,b], Martin Vestergaard[a], Arnold Skimminge[a], Lisser Rye Ejersbo[e], Thomas Z. Ramsøy[a], Christian Gerlach[e], Per Åkeson[a], Olaf B. Paulson[a,b,c], Terry L. Jernigan[a,b,c,d]

[a] Danish Research Centre for Magnetic Resonance, Copenhagen University Hospital, Hvidovre, Denmark
[b] Center for Integrated Molecular Brain Imaging, Copenhagen, Denmark
[c] Faculty of Health Sciences, University of Copenhagen, Denmark
[d] Center for Human Development, University of California, San Diego, CA, United States
[e] Learning Lab Denmark, Danish School of Education, University of Aarhus, Copenhagen, Denmark

ARTICLE INFO

Article history:
Received 24 March 2009
Received in revised form 27 August 2009
Accepted 4 November 2009
Available online 10 November 2009

Keywords:
Brain maturation
Cognitive development
Diffusion tensor imaging
Executive control
Fractional anisotropy
MRI

ABSTRACT

Cognitive control of thoughts, actions and emotions is important for normal behaviour and the development of such control continues throughout childhood and adolescence. Several lines of evidence suggest that response inhibition is primarily mediated by a right-lateralized network involving inferior frontal gyrus (IFG), presupplementary motor cortex (preSMA), and subthalamic nucleus. Though the brain's fibre tracts are known to develop during childhood, little is known about how fibre tract development within this network relates to developing behavioural control. Here we examined the relationship between response inhibition, as measured with the stop-signal task, and indices of regional white matter microstructure in typically-developing children. We hypothesized that better response inhibition performance would be associated with higher fractional anisotropy (FA) in fibre tracts within right IFG and preSMA after controlling for age. Mean FA and diffusivity values were extracted from right and left IFG and preSMA. As hypothesized, faster response inhibition was significantly associated with higher FA and lower perpendicular diffusivity in both the right IFG and the right preSMA, possibly reflecting faster speed of neural conduction within more densely packed or better myelinated fibre tracts. Moreover, both of these effects remained significant after controlling for age and whole brain estimates of these DTI parameters. Interestingly, right IFG and preSMA FA contributed additively to the prediction of performance variability. Observed associations may be related to variation in phase of maturation, to activity-dependent alterations in the network subserving response inhibition, or to stable individual differences in underlying neural system connectivity.

1. Introduction

Development of cognitive control of behaviour continues throughout childhood and adolescence (Williams, Ponesse, Schachar, Logan, & Tannock, 1999). Cognitive control of thoughts, actions, and emotions is important for normal behaviour, and deficits in behavioural control are prominent in a variety of psychiatric disorders, e.g., attention deficit/hyperactive disorder (Pliszka et al., 2006) and obsessive–compulsive disorder (Enright & Beech, 1993). In recent years, investigators have developed experimental paradigms designed to measure motor control, or more specifically the capacity to inhibit primed, or prepotent, motor responses (Chambers, Garavan, & Bellgrove, 2009). Among these is the Go/NoGo task. It is relatively easy to measure variability in the speed of a motor response using response latency; however, it is more difficult to assess the time a subject needs to inhibit a response, since no response occurs on successful "NoGo" trials. Thus, the primary measure of inhibitory function on Go/NoGo tasks is the number of errors of commission during inhibit conditions. The stop-signal task (SST) provides a more continuous measure of a subject's ability to inhibit a prepotent manual response (Logan & Cowan, 1984). The subject's task in the SST is to make a motor response to a visual target as rapidly as possible; however, on infrequent trials an acoustic "stop" signal occurs at some delay after the visual target. When the stop signal is detected, the subject must attempt to withhold, or cancel, the motor response. Obviously when the stop signal occurs very late in the trial (long stop-signal delay), the subject will not be able to inhibit the response, whereas when it occurs very soon after the visual target (short stop-signal delay), success in inhibiting the response is much more likely. The

* Corresponding author at: Danish Research Centre for Magnetic Resonance, MR-Department, Section 340, Copenhagen University Hospital, Hvidovre, Kettegaard Allé 30, 2650 Hvidovre, Denmark. Tel.: +45 3632 3323; fax: +45 3647 0302.
E-mail address: kathrine@drcmr.dk (K.S. Madsen).

0028-3932/$ – see front matter © 2009 Elsevier Ltd. All rights reserved.
doi:10.1016/j.neuropsychologia.2009.11.001

stop-signal delay is varied dynamically during the task so that the subject succeeds in inhibiting the response on stop trials approximately 50% of the time. A "stop-signal reaction time", or SSRT, is then computed for each subject by subtracting this average stop-signal delay from the median response latency for Go trials (on which no stop-signal occurs). In this way, a continuous measure is constructed of the estimated time needed to inhibit a response. Studies using the SST have implicated several brain structures in a neural network subserving response inhibition. Responding is thought to be mediated by a premotor-striatal-pallidal-motor cortical network, whereas a primarily right-lateralized network, involving prominently the inferior frontal gyrus (IFG), as well as the presupplementary motor area (preSMA), and the subthalamic nucleus (STN), has been implicated in response inhibition (Aron, Behrens, Smith, Frank, & Poldrack, 2007; Aron & Poldrack, 2006). Several functional magnetic resonance imaging (fMRI) studies have shown that inhibiting a prepotent response consistently activates prefrontal regions, particularly the right IFG, in adults (Aron et al., 2007; Aron & Poldrack, 2006; Chevrier, Noseworthy, & Schachar, 2007; Rubia, Smith, Brammer, & Taylor, 2003) as well as in children (Cohen et al., 2007). Moreover, human lesion studies suggest that the right IFG is critical for response inhibition (Rieger, Gauggel, & Burmeister, 2003), i.e., lesions in the IFG sub-region pars opercularis impair response inhibition (Aron, Fletcher, Bullmore, Sahakian, & Robbins, 2003; Aron, Robbins, & Poldrack, 2004). The latter has been confirmed in a study using transcranial magnetic stimulation, where temporary deactivation of the right pars opercularis selectively impaired the ability to stop an initiated response (Chambers et al., 2006). In addition, a recent study found that FA within the right IFG correlated with response inhibition measured with the Simon task in a small group of adults (Forstmann et al., 2008). Further, fMRI studies have found the right preSMA to be activated during stop trials (Aron et al., 2007; Aron & Poldrack, 2006). The involvement of the right preSMA in response inhibition has also been corroborated by human lesion studies (Floden & Stuss, 2006; Nachev, Wydell, O'neill, Husain, & Kennard, 2007). Moreover, weak microstimulation of neurons in the supplementary eye field improves stop task performance by delaying saccadic initiation in monkeys (Stuphorn & Schall, 2006). Another monkey study, using a switching task designed to examine control over automatic responses, found that successful switching from an automatic to a volitionally controlled response selectively increased the activity of preSMA neurons. In addition, electrical stimulation in the preSMA increased the proportion of successful switch trials (Isoda & Hikosaka, 2007). The role of the STN region in response inhibition is evidenced by fMRI studies showing this region to be activated during stop trials (Aron et al., 2007; Aron & Poldrack, 2006), and by the finding that deep-brain stimulation of the STN improves response inhibition in patients with Parkinson's disease (van den Wildenberg et al., 2006). Consistently, STN lesions impair inhibition in rodents (Eagle et al., 2008). Finally and importantly, evidence from a tractography study (Aron et al., 2007) suggests that the three regions implicated in response inhibition are interconnected. A possible preSMA-IFG connection is further supported by another tractography study in humans (Johansen-Berg et al., 2004), whereas the existence of direct fibre connections between the preSMA and STN is supported by tract tracing in monkeys (Inase, Tokuno, Nambu, Akazawa, & Takada, 1999).

Brain maturation is a complex ongoing process during childhood and early adulthood. Conventional structural MRI studies have demonstrated morphological changes in grey and white matter structures during childhood and adolescence consistent with cellular maturational processes, i.e., synaptic pruning and myelination (Giedd et al., 1999; Gogtay et al., 2004; Jernigan, Trauner, Hesselink, & Tallal, 1991; Paus et al., 1999; Sowell et al., 2004); and different grey matter structures exhibit distinct maturational trajectories (Gogtay et al., 2004; Jernigan et al., 1991; Sowell et al., 2004). Furthermore, gradual increases in global white matter volume as well as regional white matter density, have been reported in children and adolescents, possibly reflecting age-related increase in axonal diameter and ongoing myelination across this age range (Giedd et al., 1999; Paus et al., 1999, 2001). However, conventional structural MRI provides limited information about the underlying white matter microstructural properties.

Diffusion tensor imaging (DTI) measures the diffusion of water molecules in tissue. In white matter, diffusion perpendicular to highly organised fibre bundles is hindered relative to diffusion parallel to the fibres, causing diffusion anisotropy (Beaulieu, 2002). An estimate of the degree of diffusion directionality, fractional anisotropy (FA), as well as diffusivity parallel ($\lambda_{\parallel}$) and perpendicular ($\lambda_{\perp}$) to the principal diffusion direction can be derived by fitting the diffusion measurements of each voxel to the diffusion tensor model (Basser, Mattiello, & LeBihan, 1994; Beaulieu, 2002). In recent years, DTI has been applied in studies of typically-developing children and adolescents (Eluvathingal, Hasan, Kramer, Fletcher, & Ewing-Cobbs, 2007; Lebel, Walker, Leemans, Phillips, & Beaulieu, 2008; Snook, Paulson, Roy, Phillips, & Beaulieu, 2005). Age-related increases in FA have been reported in multiple locations within white matter, reflecting a disproportionate decrease in $\lambda_{\perp}$ relative to $\lambda_{\parallel}$, possibly due to ongoing myelination and/or an increase in fibre density (Eluvathingal et al., 2007; Lebel et al., 2008; Snook et al., 2005). Although the physiological significance of these changes in diffusion parameters during childhood are still not fully understood, a previous study of infants correlated increased FA (and decreased $\lambda_{\perp}$) with apparently increased neural conduction speed, as reflected in decreased latency of the first positive wave of the visual evoked potential (Dubois et al., 2008). Different white matter tracts exhibit distinct maturational patterns, with diffusion parameters in some tracts approaching adult levels earlier than others (Lebel et al., 2008).

The relationship between age-related changes in white matter microstructural properties and the concurrent development of cognitive control in children is poorly understood. White matter microstructural changes in the fronto-striatal network have been correlated with faster reaction times in the Go/NoGo task, particularly in conditions more demanding of inhibition, in a small group of children (Liston et al., 2006). However, processing factors other than inhibitory function may also influence reaction times on Go trials of the Go/NoGo task. There are currently no reports of associations between white matter microstructure and the specific measure of response inhibition from the SST, the stop-signal reaction time, in children. Here we report associations between response inhibition performance and regional white matter microstructure in typically-developing children. The major hypothesis of the study was that better response inhibition, adjusted for age, would be associated with higher FA in fiber tracts within the right IFG. Secondary hypotheses were that such relationships might also be observed for tracts in the right preSMA region. The parallel and perpendicular diffusivities were investigated to further explore the observed effects, since these diffusion parameters may provide additional information about the underlying white matter microstructure. Post-hoc analyses, including whole brain or left hemisphere region-of-interest estimates of FA and $\lambda_{\perp}$, were also performed to further explore the anatomical specificity of the effects.

2. Materials and methods

2.1. Subjects

Ninety-two typically-developing children aged 7–13 from three schools (1st–6th graders) in the Copenhagen area were inducted into the study. Prior to participation, all children assented to the procedures and informed written con-

Table 1
Demographic data for the included subjects.

	1st/2nd graders[a]	3rd/4th graders[a]	5th/6th graders[a]	All subjects
Age (mean ± SD)	8.3 ± 0.5	10.1 ± 0.3	12.2 ± 0.4	10.1 ± 1.6
Gender (female/male)	12/10	14/10	10/9	36/29
Handedness (right/left)	19/3	22/2	17/2	58/7
Parents' average years of education (mean ± SD)	13.9 ± 1.7	13.8 ± 2.0	13.7 ± 2.1	13.8 ± 1.9

Abbreviation: SD = standard deviation.
[a] Children enrolled in the study were scanned either in the months just before (when in 1st, 3rd or 5th grade) or just after (when in 2nd, 4th or 6th grade) the summer holiday.

sent was obtained from the parents/guardians after oral and written explanation of the study aims and study procedures. The study was approved by the local Danish Committee for Biomedical Research Ethics (H-KF-01-131/03), and conducted in accordance with the Declaration of Helsinki.

Twenty-seven of the participating subjects (17 girls, 10 boys) were subsequently excluded for the following reasons: incidental findings on MRI (1 subject), not completing the scanning session (3 subjects), not assessed on the SST due to failure of the response box (6 subjects), and reduced image quality as described below (17 subjects). Thus, 65 subjects were included in the present study (mean age ± std: 10.1 ± 1.6, 36 girls, 29 boys). According to a parent report, no subjects had any known history of neurological or psychiatric disorders or significant brain injury. There were no significant differences between the included and the excluded subjects on age, gender, parental education, or handedness (as assessed with the Edinburgh handedness inventory). Demographic data from the included subjects are presented in Table 1.

2.2. Stop-signal task

The stop-signal task (SST) was administered using the Cambridge Neuropsychological Test Automated Battery (Cambridge Cognition Ltd., Cambridge, UK). The SST consists of go and stop trials (Fig. 1). Subjects sit in front of a computer monitor, with each index finger resting on a response button. A circle is presented for 500 ms, followed by an arrow pointing either left or right. Subjects are instructed to press the left or right button (i.e., with the left or right index finger), depending on the direction of the arrow, without making any mistakes, and to press as fast as possible. The test consists of two parts. In the first part, there are 16 'Go' training trials without an auditory stop-signal to introduce the subjects to the press pad. In the second and longer part, an auditory stop-signal occurs in 25% of the trials. When the tone occurs, subjects must try to withhold their responses. The time between the onset of the arrow and the auditory stop signal, i.e., the stop-signal delay (SSD), changes adaptively throughout the test, depending on the subject's past performance, so that responses are inhibited successfully approximately 50% of the time for each subject. The shorter the SSD, the more likely it is that the subject will be able to inhibit his or her response. The SST is administered in 5 blocks of 64 trials. Each block is divided into four sub-blocks of 16 trials (12 go trials and 4 stop trials in random order). There is no gap between the sub-blocks and they are not evident to the subject. After each block, a feedback screen is displayed showing a histogram representation of the subject's reaction time on 'Go' trials. The histogram shown after the first block is identical for all subjects. The test administrator explains to the subject that if he/she can go faster, it will show in the next histogram, before encouraging him/her to go faster. The feedback after each of the last four blocks is the subjects' go reaction time in relation to the first block, and consists of a histogram containing the first block and the relative performance of all previous blocks. The primary behavioural outcome measure is the stop-signal reaction time (SSRT), which measures how fast subjects can inhibit a prepotent response. The SSRT is estimated using the race model (Logan & Cowan, 1984) by subtracting the SSD50, where subjects are able to inhibit 50% of their responses, from the median go RT. The race model assumes that the go and stop processes are in a race with each other and are (mainly) independent (Boucher, Palmeri, Logan, & Schall, 2007; Logan & Cowan, 1984). To get a stable estimate of the SSRT, the trials in the first half of the dataset were treated as training trials to familiarize subjects with the auditory stop-signal, and the SSRT used for statistical analysis was estimated from trials in the last half of the task.

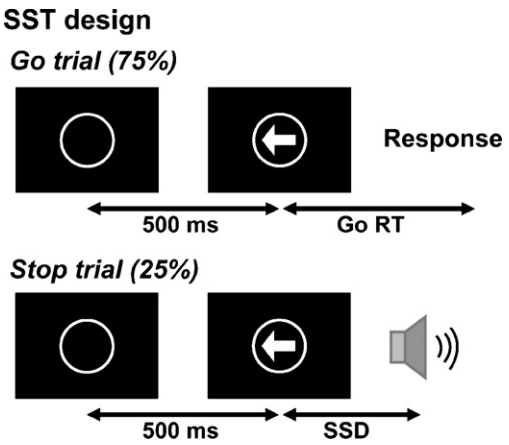

Fig. 1. The stop-signal task consists of go and stop-signal trials. A circle is presented for 500 ms, followed by a presentation of an arrow pointing either left or right. Subjects are instructed to respond as fast as possible by pressing a left or right button, depending on the direction of the arrow. In the stop trials, an auditory stop-signal occurs after the presentation of the arrow, and on these trials subjects must try to withhold their responses. The latency to the sound (the stop-signal delay [SSD]) varies dynamically throughout the study to produce the SSD50, where subjects are able to inhibit approximately 50% of their responses. The stop-signal reaction time (SSRT) is calculated as the median go RT minus the SSD50, according to the race model (Logan & Cowan, 1984).

2.3. Image acquisition

All subjects were scanned using a 3T Siemens Magnetom Trio MR scanner (Siemens, Erlangen, Germany) with an eight-channel head coil (Invivo, FL, USA). Subjects were scanned the same day as the SST was administered. All acquired scans were aligned parallel to the anterior commisure–posterior commisure (AC–PC) line. Diffusion-weighted (DW) images of the whole brain were acquired using a twice-refocused balanced spin echo sequence that minimised eddy current distortion (Reese, Heid, Weisskoff, & Wedeen, 2003). Ten non-DW images ($b = 0$) and 61 DW images, encoded along independent collinear diffusion gradient orientations (Cook, Symms, Boulby, & Alexander, 2007; Jansons & Alexander, 2003), were acquired with a b value of 1200 s/mm^2 (TR = 8200 ms; TE = 100 ms, FOV = 220 mm × 220 mm, matrix = 96 × 96, GRAPPA: acceleration factor = 2; number of reference lines = 48, 61 transverse slices with no gap, 2.3 mm × 2.3 mm × 2.3 mm voxels, NEX = 1, acquisition time = 9.50 min). A gradient echo based field map sequence (TR = 530 ms, TE[1] = 5.19 ms and TE[2] = 7.65 ms, FOV = 256 mm × 256 mm; matrix = 128 × 128, 47 transverse slices with no gap, voxel size = 2 mm × 2 mm × 3 mm, NEX = 1, acquisition time = 2.18 min) was acquired to correct geometric distortions caused by B_0 magnetic field inhomogeneities. T_2-weighted images of the whole head were acquired using a 3D turbo spin echo sequence (TR = 3000 ms, TE = 354 ms, FOV = 282 mm × 282 mm, matrix = 256 × 256, 192 sagittal slices with no gap, 1.1 mm × 1.1 mm × 1.1 mm voxels, NEX = 1, acquisition time = 8.29 min) for generating brain masks. T_1-weighted and proton density weighted images were also acquired in the imaging session, but these images were not used in the analysis reported here.

2.4. Image evaluation

All subjects' images were evaluated by an experienced neuroradiologist. Prior to image analysis, and blind to behavioural data, the raw images from all subjects were visually checked to ascertain the quality of the data. As described above, based on this inspection, 17 subjects had significantly reduced image quality due to movement or susceptibility artefacts and were excluded from further analysis.

2.5. Image analysis

Images were preprocessed using pipelines implemented in Matlab, using mainly SPM2 routines. DW images were oriented to the MNI coordinate system and corrected for geometric distortions due to B_0 inhomogeneities. The first B_0 image was coregistered to MNI space using a rigid transformation (6 parameter mutual information), after which all DW images were coregistered (no reslicing) to the first B_0 image. Next, all coregistered images were corrected for geometric distortions using the acquired B_0 field map (Andersson, Hutton, Ashburner, Turner, & Friston, 2001) and resliced into the MNI coordinate system using trilinear interpolation. Note that

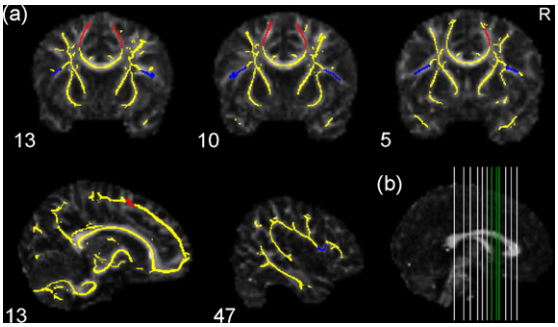

Fig. 2. (a) Coronal and sagittal slices of the mean skeleton (yellow) overlaid on the target FA image. The blue segments are the IFG (inferior frontal gyrus, pars opercularis) ROIs and the red segments are the preSMA (presupplementary motor area) ROIs. (b) Midsagittal view showing the planes (in green) of the three coronal sections in the top row. The planes indicated in white and green represent the coronal views of the effect-size maps shown in Figs. 3 and 4.

this procedure involves only one reslicing step. The diffusion tensor was fitted using the RESTORE algorithm (Chang, Jones, & Pierpaoli, 2005) implemented in Camino (Cook et al., 2006), and FA, $\lambda_{\parallel}$ (λ_1) and $\lambda_{\perp}((\lambda_2+\lambda_3)/2)$ were calculated. A brain mask based on the T_2-weighted image was automatically created using SPM2 segmentation routines and morphological operations and applied to the FA and diffusivity images.

Because our hypotheses relate to the degree of anisotropy in specific fibre tracts, we used a region-of-interest (ROI) approach to extract FA and diffusivity measures from specific ROIs for each subject. However, we first used tract-based spatial statistics (TBSS) (Smith et al., 2006) to accomplish spatial normalisation and to align the fibre tracts across children. Specifically, FSL 4.0.1 (Smith et al., 2004) was used to align all subjects' FA images into a common space using the nonlinear registration IRTK (Rueckert et al., 1999). A study-specific target, the group's most representative FA image, was identified by aligning each subject's FA image to every other subject's FA image. The target FA image was aligned to 1 mm^3 MNI space using affine registration, and subsequently all subjects' FA images were then aligned to this study-specific target FA image. A cross-subject mean FA image was created and thinned to create a mean FA skeleton, representing the centres of all tracts common to the group. The mean FA skeleton was thresholded at FA > 0.25, and contained 103,503 1 mm^3 interpolated isotropic voxels, corresponding to approximately one quarter of the voxels with FA above 0.25. Each subject's aligned FA image was then projected onto the study-specific skeleton by locating the voxels with the highest local FA value in the direction perpendicular to the skeleton tracts and assigning the value of these voxels to the skeleton at this standardised location. Note that this results in a mapping of each voxel location in the skeleton to a specific voxel in the individual FA maps. In addition, the nonlinear warps and the skeleton projections were applied to the $\lambda_{\parallel}$ and $\lambda_{\perp}$ data.

2.6. Regions-of-interest

Regions-of-interest (ROIs) were drawn onto the study-specific skeleton overlaid on the target FA map. Since the TBSS procedure projects individual FA values and other DTI derived parameters onto a common framework, i.e., the mean study-specific skeleton, one can extract each subject's individual measures directly by delineating a ROI once. The ROIs were placed in the right and left IFG (pars opercularis) and in the right and left preSMA (Fig. 2). The right and left pars opercularis were located using a brain atlas (Duvernoy, 1999) and published information about the morphology of the pars opercularis (Tomaiuolo et al., 1999). The boundaries of the IFG ROIs were found by using anatomical information visible in the target FA map, where the vertical ramus of the lateral fissure and the inferior part of the precentral sulcus, indicated by low FA values, were used as landmarks to define the anterior and posterior boundaries of the pars opercularis. The skeleton defined the superior boundary, in that the lateral part of the pars opercularis segment was perpendicular to the segment going into the pars triangularis. The right IFG ROI contained 379 voxels and the left contained 322 voxels. The location of the preSMA ROIs was based on MNI coordinates derived from published functional and structural studies (Behrens, Jenkinson, Robson, Smith, & Johansen-Berg, 2006; Johansen-Berg et al., 2004), and defined between MNI $x = 0$ and $x = 20$. However, based on the anatomical information provided by the target FA map, the posterior and anterior boundaries were set to MNI $x = 5$ and $x = 14$ for the right and $x = 6$ and $x = 15$ for the left preSMA ROI, respectively. The right preSMA ROI included 295 voxels and the left ROI included 311 voxels. Mean FA, $\lambda_{\parallel}$ and $\lambda_{\perp}$ values from all four ROIs and the whole skeleton were extracted for each subject for statistical analyses. We initially attempted to include a ROI in the internal capsule, given that the subthalamic nucleus (STN) has been implicated in response inhibition (Aron & Poldrack, 2006; van den Wildenberg et al., 2006) and fibre tracts connecting the IFG and preSMA with the STN have been found (Aron et al., 2007). However, due to the lack of clear landmarks delimiting the relevant segments of the internal capsule, it was deemed not feasible to define an appropriate ROI on the mean skeleton.

2.7. Statistical analysis

The statistical analyses were performed with SPSS 15.0 using multiple linear regression models predicting SSRT. Multicollinearity between the predictors was assessed for all models. The statistical tests were performed hierarchically. The major hypotheses that right IFG FA and right preSMA, adjusted for age, would be significantly and negatively associated with SSRT were tested with $\alpha = 0.025$. Planned follow-up analyses were contingent on observing significant associations with FA in the primary analyses. Follow-up analyses were done to assess the anatomical specificity of the effects, either by adjusting for the whole skeleton FA or by adjusting for the corresponding left hemisphere ROI FA. The parallel and perpendicular diffusivities were investigated to further explore the nature of these observed effects by following the same statistical analysis protocol as for the FA data. An additional follow-up analysis was conducted to predict SSRT with the right IFG FA and the right preSMA FA measures simultaneously. Exploratory models including either gender or age by gender interaction effects revealed no significant gender effects and, thus, models presented do not include gender.

Two effect-size maps are presented to provide further anatomical information about the association between FA and SSRT (Jernigan, Gamst, Fennema-Notestine, & Ostergaard, 2003). The effect-size maps are *t*-maps of the correlation between FA and SSRT, however the sign of the correlations are reversed so that correlations between high FA and better response inhibition performance (lower reaction time) are shown in warm colours (red to yellow). The maps are presented with and without adjusting for age, respectively. The *t*-maps were generated using the Monte Carlo permutation test with 10,000 permutations implemented in the randomise program within FSL (Nichols & Holmes, 2002).

3. Results

Behavioural measures for the SST and the FA measures for the four ROIs are presented in Table 2. The subjects inhibited approximately 50% of their responses in the stop trials, indicating that the adaptive tracking algorithm performed as expected. Separate statistics are provided for boys and girls, but no gender differences approached significance (*P*s > 0.37).

Table 2
Behavioural measures of the SST and fractional anisotropy measures of the region-of-interest.*.

Behavioural measure	All subjects	Girls	Boys
Median correct Go RT (ms)	504.4 ± 103.5	510.3 ± 114.1	497.0 ± 90.2
Mean SSD 50% (ms)	287.1 ± 104.9	297.5 ± 109.0	274.1 ± 99.9
Percentage inhibition	50.5 ± 0.1	50.9 ± 0.1	49.9 ± 0.1
SSRT (ms)	217.3 ± 60.4	212.9 ± 59.1	222.8 ± 62.5
Region-of-interest	**All subjects FA**	**Girls FA**	**Boys FA**
Right IFG	0.405 ± 0.025	0.404 ± 0.026	0.407 ± 0.024
Right preSMA	0.435 ± 0.034	0.435 ± 0.034	0.436 ± 0.034
Left IFG	0.411 ± 0.031	0.414 ± 0.030	0.407 ± 0.331
Left preSMA	0.444 ± 0.024	0.442 ± 0.027	0.446 ± 0.021

Abbreviations: SST = stop-signal task, SD = standard deviation, RT = reaction time, SSRT = stop-signal reaction time, SSD = stop-signal delay.
* All values are Mean ± SD.

Table 3
Linear regression models predicting SSRT from FA: *a priori* hypotheses.[a].

		Right IFG		Right preSMA		Age	
Model	R^2	β	P	β	P	β	P
[1]	0.192	−0.396	0.00024			−0.420	0.00011
[2]	0.367			−0.319	0.0038	−0.416	0.00023
[3]	0.142	−0.438	0.00026				
[4]	0.312			−0.377	0.002		
[5]	0.257	−0.356	0.0029	−0.268	0.023		
[6]	0.441	−0.330	0.0022	−0.221	0.037	−0.396	0.00018

Each model is referred to with a number in the leftmost column, representing the models: [1] right IFG FA, adjusted for age; [2] right preSMA FA, adjusted for age; [3] right IFG FA; [4] right preSMA FA; [5] right IFG and right preSMA FA; [6] right IFG and right preSMA, adjusted for age. Models [1] and [2] test the *a priori* hypotheses (see text for details). *Abbreviations*: SSRT = stop-signal reaction time, IFG = inferior frontal gyrus, PreSMA = presupplementary motor area, and FA = fractional anisotropy.

[a] Linear regression models are presented in rows. Predictors are presented in columns.

3.1. Associations between SSRT and DTI parameters within IFG and preSMA

Results for the primary and secondary hypotheses are presented in Table 3, where each row represents a separate, planned model predicting SSRT. As hypothesized, right IFG FA, adjusted for age, was significantly and negatively associated with SSRT (Fig. 3a and Table 3, model 1), indicating that better response inhibition is associated with higher mean FA values within the right IFG. A similar significant relationship was observed for right preSMA FA (Fig. 3b and Table 3, model 2). When not controlling for age, which itself was significantly and negatively correlated with SSRT ($R^2 = 0.212$, $\beta = -0.460$, $P = 0.0001$) the effects were slightly larger (Table 3, models 3 and 4). Interestingly, when entered as predictors simultaneously, either alone or adjusting for age, both right IFG and preSMA FA remained significant predictors of SSRT (Table 3, models 5 and 6), suggesting that these effects are additive.

Results from follow-up analyses of the FA data, testing for the anatomical specificity of the above-mentioned effects, are presented in Table 4. When adjusting for age and whole skeleton FA, right IFG FA as well as right preSMA FA remained significant predictors of SSRT (Table 4, models 1 and 3), suggesting that the association between SSRT and right IFG and preSMA FA were not mediated by global increase in FA. In both models, the additional effect of whole skeleton FA did not reach significance, though whole skeleton FA, adjusted for age, was itself significantly and negatively associated with SSRT ($R^2 = 0.288$, $\beta = -0.304$, $P = 0.013$). Furthermore, the right hemisphere FA values remained significant when controlling for age and the corresponding left hemisphere ROI FA values (Table 4, models 2 and 4). The additional contributions of the latter did not approach significance in either case. Although left IFG FA by itself was correlated with SSRT ($R^2 = 0.075$, $P = 0.028$), this association was not significant after controlling for age ($P = 0.09$), and left preSMA FA did not exhibit a significant association with SSRT ($P = 0.62$).

The parallel and perpendicular diffusivities were investigated to further explore the nature of these effects. Both right IFG and preSMA $\lambda_\perp$ were significantly and positively associated with SSRT alone (Table 5, models 1 and 5) or when controlling for age (Table 5, models 2 and 6) or for left hemisphere ROI $\lambda_\perp$ (Table 5, models 4 and 8). When controlling for both age and whole skeleton $\lambda_\perp$, the effect of right IFG $\lambda_\perp$ remained significant, though the effect of right preSMA $\lambda_\perp$ did not (Table 5, models 3 and 7, respectively). Whole skeleton $\lambda_\perp$, adjusted for age, was significantly and positively related with SSRT ($R^2 = 0.307$, $\beta = 0.333$, $P = 0.005$). These effects contrasted with those for parallel diffusivity. Neither right IFG $\lambda_\parallel$ nor right preSMA $\lambda_\parallel$ was significantly associated with SSRT, with or without adjusting for age ($P > 0.5$). However, whole skeleton $\lambda_\parallel$ adjusted for age was significantly and positively correlated with SSRT ($R^2 = 0.267$, $\beta = 0.242$, $P = 0.035$).

Collinearity diagnostics were performed for all of the regression models and multicollinearity among the explanatory variables in the models was low (tolerance = 0.46–0.99, variance inflation factor = 1.01–2.17).

3.2. Effect-size map

The present study was designed to test specific anatomical hypotheses about the relationship between right IFG and preSMA fibre tract microstructure and variability in SST performance in children. Therefore neither a whole brain, voxel-wise analysis of the effects (appropriately adjusted for test-multiplicity), nor a restricted voxel-wise analysis with small volume correction was deemed appropriate for testing these *a priori* hypotheses. However, since the analysis we used produces estimates of the effect size at each voxel, we have provided visualisation of the effect-size

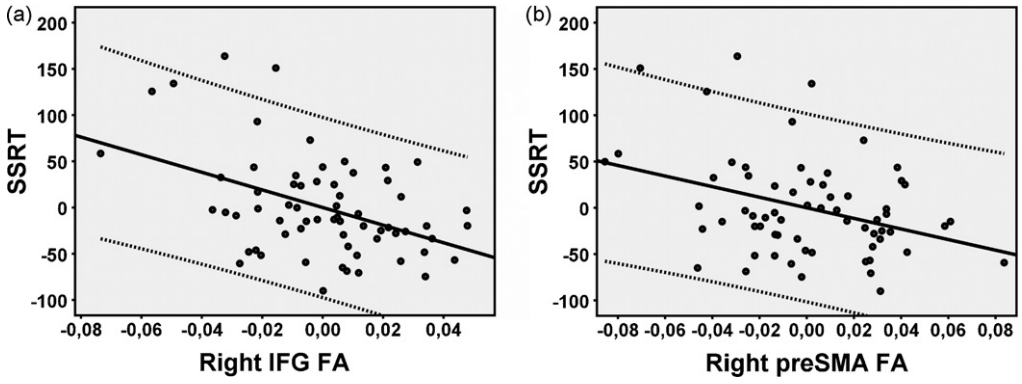

Fig. 3. Partial regression plots of the stop-signal reaction time (SSRT) as a function of (a) right inferior frontal gyrus (IFG) FA, adjusted for age and (b) right presupplementary motor area (preSMA) FA, adjusted for age.

Table 4
Linear regression models predicting SSRT from FA: follow-up analyses.[a].

		Right IFG		Age		Whole skeleton		Left IFG	
Model	R^2	β	P	β	P	β	P	β	P
[1]	0.383	−0.339	0.0032	−0.361	0.0019	−0.153	0.214		
[2]	0.372	−0.372	0.00099	−0.409	0.00020			−0.076	0.486
		Right PreSMA		Age		Whole skeleton		Left PreSMA	
Model	R^2	β	P	β	P	β	P	β	P
[3]	0.334	−0.243	0.044	−0.349	0.0037	−0.183	0.162		
[4]	0.328	−0.367	0.0019	−0.431	0.00015			0.137	0.231

Each model is referred to with a number in the leftmost column, representing the models: [1,3] right ROI, adjusted for age and whole skeleton FA; [2,4] right ROI, adjusted for age and corresponding left ROI FA. *Abbreviations*: SSRT = stop-signal reaction time, IFG = inferior frontal gyrus, PreSMA = presupplementary motor area, and FA = fractional anisotropy.

[a] Multiple linear regression models are presented in rows. Predictors are presented in columns.

maps. These maps show the distribution of *t*-values in skeleton voxels, and are presented to provide additional information about the anatomical distribution of associations between response inhibition performance and FA in white matter. Two maps are provided, the first (Fig. 4) displaying the association between FA and SSRT controlling for age, and the second (Fig. 5) displaying the direct association of FA and SSRT. The contrast has been coded so that association of lower SSRT (better response inhibition) with higher FA yields positive *t*-values. Increasing positive *t*-values are shown in warm colours ranging from red to yellow, whereas decreasing negative *t*-values are shown in cool colours ranging from dark blue to light blue. The position of the depicted coronal slices is indicated in Fig. 2b. Slices 5, 10, and 13 are through the ROI locations and are the same as those shown in Fig. 2a, top row. Slice 18 shows the effects in the hand area in the motor cortex. In general, the associations between higher FA and better response inhibition appear to be modestly stronger when not correcting for age. In Fig. 6, sagittal views of the effect-size map show clusters of voxels with relatively high *t*-values within the internal capsule. Some clusters appear to be located in the posterior limb of the internal capsule.

4. Discussion

The present study examined associations between response inhibition performance and white matter microstructure within IFG (pars opercularis) and preSMA in children aged 7–13 years. As hypothesized, higher FA in fibre tracts within right IFG and preSMA was significantly associated with better response inhibition. Since both FA (Lebel et al., 2008) and response inhibition (Williams et al., 1999) increase throughout childhood and adolescence, a correlation between these measures could represent a nonspecific association attributable to unmeasured factors indexed by chronological age. For example, since height also increases in children over this age range, one might expect to find a simple correlation between height and response inhibition within a group of children with varying ages. However, since height has little direct relationship to cognitive functioning in children, one would expect the correlation between these variables to be substantially reduced after controlling for age statistically. Thus, we hypothesized that the associations between SSRT and FA within the right IFG and preSMA would remain significant after controlling for age; i.e., that even among children of similar age, those with higher FA in right IFG and right preSMA would exhibit stronger response inhibition performance. These hypotheses were confirmed.

Several planned follow-up analyses were conducted to explore the nature of these associations. We were interested to assess the anatomical specificity of the associations between response inhibition performance and fibre structure within the right IFG and preSMA, i.e., the extent to which response inhibition exhibited a relatively specific relationship to FA in this fibre tract relative to others. This is an important question, since it is known that FA increases concurrently in many fibre tracts during childhood (Lebel et al., 2008). Mean FA for the whole skeleton, adjusted for age, was modestly correlated with SSRT, suggesting that global individual differences in white matter microstructure between children of similar age are mediating this association. However, the effects on SSRT of FA in the right IFG and in the right preSMA remained significant when this global measure of FA was included as a

Table 5
Linear regression models predicting SSRT from $\lambda_\perp$: follow-up analyses.[a].

		Right IFG		Age		Whole skeleton		Left IFG	
Model	R^2	β	P	β	P	β	P	β	P
[1]	0.244	0.506	0.000017						
[2]	0.378	0.419	0.00014	−0.360	0.00090				
[3]	0.380	0.379	0.0097	−0.346	0.0024	0.063	0.674		
[4]	0.378	0.404	0.0013	−0.355	0.0014			0.251	0.803
		Right PreSMA		Age		Whole skeleton		Left PreSMA	
Model	R^2	β	P	β	P	β	P	β	P
[5]	0.147	0.383	0.0016						
[6]	0.303	0.308	0.0059	−0.403	0.00042				
[7]	0.331	0.191	0.145	−0.342	0.0037	0.218	0.118		
[8]	0.305	0.337	0.011	−0.409	0.00042			−0.055	0.672

Each model is referred to with a number in the leftmost column, representing the models: [1,5] right ROI $\lambda_\perp$; [2,6] right ROI $\lambda_\perp$, adjusted for age; [3,7] right ROI $\lambda_\perp$, adjusted for age and whole skeleton $\lambda_\perp$; [4,8] right ROI $\lambda_\perp$, adjusted for age and corresponding left ROI $\lambda_\perp$. *Abbreviations*: SSRT = stop-signal reaction time, IFG = inferior frontal gyrus, PreSMA = presupplementary motor area, and $\lambda_\perp$ = perpendicular diffusivity.

[a] Linear regression models are presented in rows. Predictors are presented in columns.

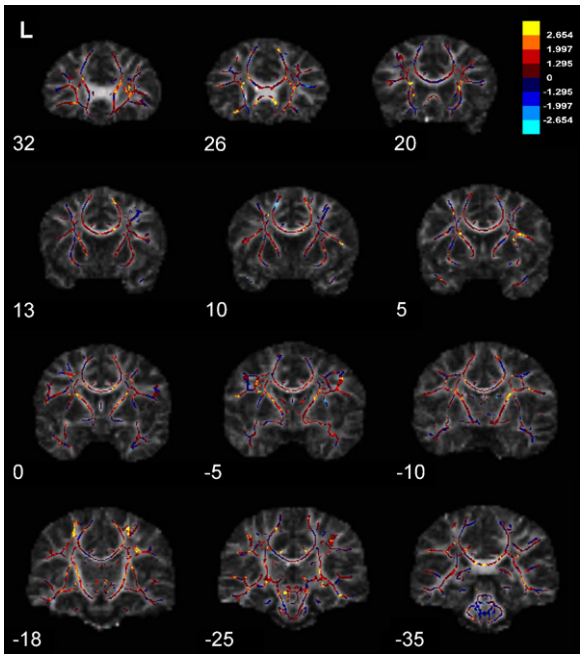

Fig. 4. Effect-size map of the negative association between SSRT and FA adjusted for age. The effect-size map is overlaid on the target FA image. The colour bar shows the mapping of colours to the values of the *t*-statistics. All voxels on the skeleton are coloured. Images are shown with the subject's right side on the right side (neurological convention). The MNI coordinates for the coronal images are given under each image. The IFG and preSMA ROIs were located in slice 5, 10 and 13 (see Fig. 2a, top row).

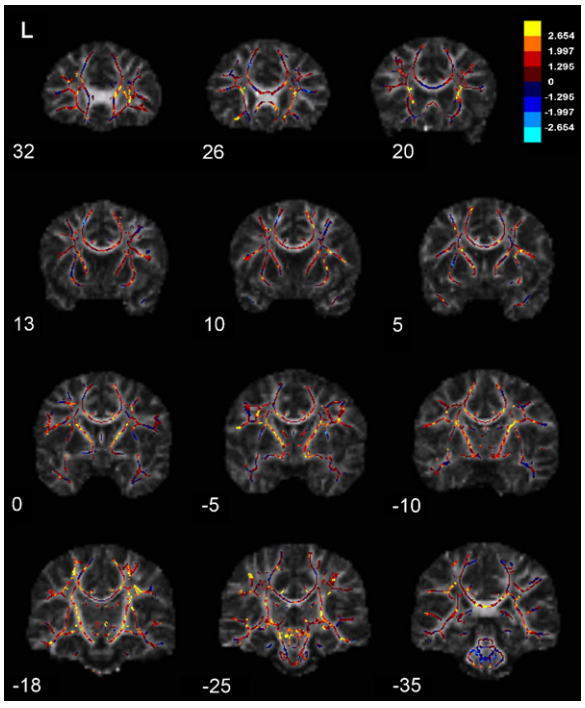

Fig. 5. Effect-size map of the negative association between SSRT and FA. The effect-size map is overlaid on the target FA image. The colour bar shows the mapping of colours to the values of the *t*-statistics. All voxels on the skeleton are coloured. Images are shown with the subject's right side on the right side (neurological convention). The MNI coordinates for the coronal images are given under each image. The IFG and preSMA ROIs were located in slice 5, 10 and 13 (see Fig. 2a, top row).

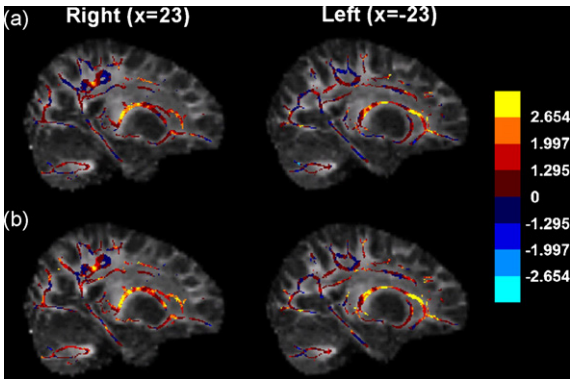

Fig. 6. Effect-size map of the negative association between SSRT and FA with (a) and without (b) adjusting for age. The effect-size map is overlaid on the target FA image. The colour bar shows the mapping of colours to the values of the *t*-statistics. All voxels on the skeleton are coloured. The sagittal slices were selected to show clusters of voxels with relatively high *t*-values within the internal capsule. The MNI coordinates for the images are given above the images.

covariate, and in these models the effect of the global measure no longer approached significance. This suggests that the relationships between response inhibition and FA within the right IFG and preSMA are not likely to be mediated by global white matter FA differences and may be more strongly related to the structure in specific tracts. Moreover, results from similar analysis controlling for FA in the left hemisphere ROIs, suggested that the effects of structure in the right hemisphere tracts were more robust than effects of structure in the left hemisphere tracts. This pattern is consistent with a significant degree of anatomical specificity of the effects relating FA and SSRT performance; and it is consistent with previous studies suggesting that a primarily right-lateralized network involving IFG and preSMA mediates response inhibition (Aron et al., 2007, 2003; Chambers et al., 2006; Floden & Stuss, 2006; Nachev et al., 2007). Interestingly, when predicting SSRT performance with right IFG and right preSMA FA simultaneously (with or without adjusting for age), both regions remained significant predictors. This suggests that increased FA in fibre tracts within the right IFG and right preSMA may contribute additively to better response inhibition performance.

TBSS improves inter-subject registration of brain fibre tracts relative to prior methods for performing spatial normalisation of FA images (Smith et al., 2006) and the method obviates the need for extensive spatial smoothing. Thus, the use of TBSS in the present study aimed to increase the sensitivity of our ROI approach relative to ROI methods used in previous DTI studies in children. We averaged FA over the segments of the tract skeleton that corresponded to the expected location of the targeted tracts after applying TBSS to align the tracts across subjects. This was considered to be a more objective way of estimating FA within a comparable portion of the tract within each individual than subjective (manual) delineation of regions within the white matter, and a more powerful test of our hypothesis than a voxel-wise approach. However, the method produces only an approximation of FA in the targeted tracts, and in future studies it may be possible to employ better validated tractography methods that define the tracts based on connectivity, or new methods using probabilistic atlases (Hagler et al., 2009) to more definitively assess the structure in particular fibre tracts.

We performed additional analyses of parallel and perpendicular diffusivities to further investigate the effects found in the right IFG and preSMA, since these diffusion parameters may provide additional information about the underlying white matter microstructure. We found a similar relationship between SSRT and $\lambda_{\perp}$ to that observed with FA in the fibre tracts within the right IFG and preSMA. The effects of $\lambda_{\parallel}$ appeared weaker and were

not significant. This suggests that the increase in FA associated with better response inhibition performance is mainly driven by decreased $\lambda_\perp$. Although interpretation of changes in DTI parameters is not straightforward, previous studies suggest that $\lambda_\perp$ may be more sensitive to changes in myelination (Song et al., 2003, 2005). Using a mouse model of retinal ischemia, a DTI and histology study revealed a gradual decrease in relative anisotropy, caused by, at first, decrease in $\lambda_\parallel$, corresponding with the timing of axonal degeneration, followed by increase in $\lambda_\perp$, associated with optic nerve demyelination (Song et al., 2003). Another rodent study, using a model of experimental de- and remyelination of the corpus callosum, found that continuous cuprizone (neurotoxin) treatment caused demyelination of the callosal fibres, reflected by increased $\lambda_\perp$. When the treatment was discontinued, the effects were reversed, and the progression of fibre remyelination was consistent with decrease in $\lambda_\perp$ (Song et al., 2005). Although $\lambda_\perp$ does not measure myelin directly, these findings suggest that the degree of myelination may be contributing to the observed effects in the present study. Age-related FA increases in fibre tracts have been linked to decreases in $\lambda_\perp$ in previous studies (Lebel et al., 2008). However, other tissue parameters, such as axonal diameter, packing density, spacing, or number; extracellular volume fraction; or tract geometry may also contribute to changes in FA and $\lambda_\perp$ (Beaulieu, 2002; Madler, Drabycz, Kolind, Whittall, & MacKay, 2008; Schwartz et al., 2005).

Previous studies have linked the STN to response inhibition (Aron & Poldrack, 2006; van den Wildenberg et al., 2006), and fibre tracts connecting the IFG and preSMA with STN pass through the internal capsule (Aron et al., 2007). Due to the lack of clear landmarks delimiting these fibres within the internal capsule, we were not able to define an appropriate ROI in the internal capsule that distinguished these tracts. However, in the effect-size maps displaying the associations between higher FA and better response inhibition performance, clusters with relatively high *t*-values were observed in the internal capsule (Fig. 6). Though it is not possible to conclude whether or not these connections are contained in the observed clusters, the pattern observed in the effect-size maps suggests that the internal capsule may be an important part of the neural circuit mediating variability in response inhibition in this study. Future studies employing tractography may provide additional evidence.

As mentioned above, these findings suggest that even among children of similar age, higher FA and lower $\lambda_\perp$ in right IFG and preSMA are associated with better response inhibition performance. Many questions remain about what such age-adjusted variability in FA and $\lambda_\perp$ might represent. It may reflect individual differences in trajectories of fibre tract maturation of the neural system subserving response inhibition, i.e., differences in the phase of IFG and preSMA development among children of similar age. It is plausible that this variability could mediate, at least to some extent, the association between response inhibition performance and white matter microstructure found in the present study, since both white matter structure (Lebel et al., 2008) and inhibitory control (Williams et al., 1999) continue to develop across this age range. Alternatively, it could represent individual differences in the structure of the fibre tracts (perhaps reflecting differences in the underlying neural system connectivity) that emerge earlier during brain development and remain stable in spite of superimposed biological changes associated with development. This is plausible since individual differences in behavioural performance have been associated with FA variability in adults (Forstmann et al., 2008; Gold, Powell, Xuan, Jiang, & Hardy, 2007; Wolbers, Schoell, & Buchel, 2006) as well as children.

It is also plausible that the difference in microstructure of the fibre tracts are influenced by dynamic processes, possibly associated with activity levels in the neural circuits. In a recent DTI study, accelerated white matter development (higher FA) in the sagittal stratum was found in preterm relative to full-term infants at term equivalent age, possibly as a result of increased intensity of sensorimotor stimulation associated with extrauterine life (Gimenez et al., 2008). Thus, the differences observed in the present study could reflect variability in the experiences and learning of the children. Finally, genetic variability may play a role in mediating these differences.

5. Conclusion

FA and $\lambda_\perp$ within the right IFG and preSMA exhibit associations with SSRT that are not attributable to age and the associations do not appear to reflect behavioural effects of global white matter development. Further, the contributions of right IFG and preSMA FA to the prediction of response inhibition appear to be additive. Children may vary in the phase of maturation in the network subserving response inhibition, and this variability may mediate the associations. Alternatively, the associations could be mediated by individual differences among the children in underlying neural system connectivity, or to more transient differences associated with dynamic (perhaps activity-dependent) processes. Longitudinal observations are needed to help distinguish between these, and other, possibilities.

Acknowledgements

This work was supported by the Danish Medical Research Council, University of Copenhagen's Research Priority Area Body and Mind, and the Lundbeck Foundation.

References

Andersson, J. L., Hutton, C., Ashburner, J., Turner, R., & Friston, K. (2001). Modeling geometric deformations in EPI time series. *Neuroimage*, *13*, 903–919.
Aron, A. R., Behrens, T. E., Smith, S., Frank, M. J., & Poldrack, R. A. (2007). Triangulating a cognitive control network using diffusion-weighted magnetic resonance imaging (MRI) and functional MRI. *Journal of Neuroscience*, *27*, 3743–3752.
Aron, A. R., Fletcher, P. C., Bullmore, E. T., Sahakian, B. J., & Robbins, T. W. (2003). Stop-signal inhibition disrupted by damage to right inferior frontal gyrus in humans. *Nature Neuroscience*, *6*, 115–116.
Aron, A. R., & Poldrack, R. A. (2006). Cortical and subcortical contributions to Stop signal response inhibition: Role of the subthalamic nucleus. *Journal of Neuroscience*, *26*, 2424–2433.
Aron, A. R., Robbins, T. W., & Poldrack, R. A. (2004). Inhibition and the right inferior frontal cortex. *Trends in Cognitive Sciences*, *8*, 170–177.
Basser, P. J., Mattiello, J., & LeBihan, D. (1994). MR diffusion tensor spectroscopy and imaging. *Biophysical Journal*, *66*, 259–267.
Beaulieu, C. (2002). The basis of anisotropic water diffusion in the nervous system—A technical review. *NMR in Biomedicine*, *15*, 435–455.
Behrens, T. E., Jenkinson, M., Robson, M. D., Smith, S. M., & Johansen-Berg, H. (2006). A consistent relationship between local white matter architecture and functional specialisation in medial frontal cortex. *Neuroimage*, *30*, 220–227.
Boucher, L., Palmeri, T. J., Logan, G. D., & Schall, J. D. (2007). Inhibitory control in mind and brain: An interactive race model of countermanding saccades. *Psychological Review*, *114*, 376–397.
Chambers, C. D., Bellgrove, M. A., Stokes, M. G., Henderson, T. R., Garavan, H., Robertson, I., et al. (2006). Executive "brake failure" following deactivation of human frontal lobe. *Journal of Cognitive Neuroscience*, *18*, 444–455.
Chambers, C. D., Garavan, H., & Bellgrove, M. A. (2009). Insights into the neural basis of response inhibition from cognitive and clinical neuroscience. *Neuroscience and Biobehavioral Review*, *33*, 631–646.
Chang, L. C., Jones, D. K., & Pierpaoli, C. (2005). RESTORE: Robust estimation of tensors by outlier rejection. *Magnetic Resonance in Medicine*, *53*, 1088–1095.
Chevrier, A. D., Noseworthy, M. D., & Schachar, R. (2007). Dissociation of response inhibition and performance monitoring in the stop signal task using event-related fMRI. *Human Brain Mapping*, *28*, 1347–1358.
Cohen, J. R., Sabb, F. W., Bilder, R. M., Bookheimer, S. Y., Knowlton, B. J., Asarnow, R. F., et al. (2007). Neural substrates of response inhibition in children examined with fMRI. 13th annual meeting of the organization of human brain mapping. *Neuroimage*, *36*(Suppl. 1).
Cook, P. A., Bai, Y., Nedjati-Gilani, S., Seunarine, K. K., Hall, M. G., Parker, G. J., et al. (2006). Camino: Open-source diffusion-MRI reconstruction and processing. In *14th scientific meeting of the international society for magnetic resonance in medicine* Seattle, WA, USA, (p. 2759).
Cook, P. A., Symms, M., Boulby, P. A., & Alexander, D. C. (2007). Optimal acquisition orders of diffusion-weighted MRI measurements. *Journal of Magnetic Resonance Imaging*, *25*, 1051–1058.

Dubois, J., Dehaene-Lambertz, G., Soares, C., Cointepas, Y., Le Bihan, D., & Hertz-Pannier, L. (2008). Microstructural correlates of infant functional development: Example of the visual pathways. *Journal of Neuroscience*, *28*, 1943–1948.

Duvernoy, H. M. (1999). *The human brain; surface, blood supply and three-dimensional section anatomy* (2nd ed.). Wien: Springer.

Eagle, D. M., Baunez, C., Hutcheson, D. M., Lehmann, O., Shah, A. P., & Robbins, T. W. (2008). Stop-signal reaction-time task performance: Role of prefrontal cortex and subthalamic nucleus. *Cerebral Cortex*, *18*, 178–188.

Eluvathingal, T. J., Hasan, K. M., Kramer, L., Fletcher, J. M., & Ewing-Cobbs, L. (2007). Quantitative diffusion tensor tractography of association and projection fibers in normally developing children and adolescents. *Cerebral Cortex*, *17*, 2760–2768.

Enright, S. J., & Beech, A. R. (1993). Reduced cognitive inhibition in obsessive–compulsive disorder. *British Journal of Clinical Psychology*, *32*(Pt 1), 67–74.

Floden, D., & Stuss, D. T. (2006). Inhibitory control is slowed in patients with right superior medial frontal damage. *Journal of Cognitive Neuroscience*, *18*, 1843–1849.

Forstmann, B. U., Jahfari, S., Scholte, H. S., Wolfensteller, U., van den Wildenberg, W. P., & Ridderinkhof, K. R. (2008). Function and structure of the right inferior frontal cortex predict individual differences in response inhibition: A model-based approach. *Journal of Neuroscience*, *28*, 9790–9796.

Giedd, J. N., Blumenthal, J., Jeffries, N. O., Castellanos, F. X., Liu, H., Zijdenbos, A., et al. (1999). Brain development during childhood and adolescence: A longitudinal MRI study. *Nature Neuroscience*, *2*, 861–863.

Gimenez, M., Miranda, M. J., Born, A. P., Nagy, Z., Rostrup, E., & Jernigan, T. L. (2008). Accelerated cerebral white matter development in preterm infants: A voxel-based morphometry study with diffusion tensor MR imaging. *Neuroimage*, *41*, 728–734.

Gogtay, N., Giedd, J. N., Lusk, L., Hayashi, K. M., Greenstein, D., Vaituzis, A. C., et al. (2004). Dynamic mapping of human cortical development during childhood through early adulthood. *Proceedings of the National Academy of Sciences United States of America*, *101*, 8174–8179.

Gold, B. T., Powell, D. K., Xuan, L., Jiang, Y., & Hardy, P. A. (2007). Speed of lexical decision correlates with diffusion anisotropy in left parietal and frontal white matter: Evidence from diffusion tensor imaging. *Neuropsychologia*, *45*, 2439–2446.

Hagler, D. J., Jr., Ahmadi, M. E., Kuperman, J., Holland, D., McDonald, C. R., Halgren, E., et al. (2009). Automated white-matter tractography using a probabilistic diffusion tensor atlas: Application to temporal lobe epilepsy. *Human Brain Mapping*, *30*(5), 1535–1547.

Inase, M., Tokuno, H., Nambu, A., Akazawa, T., & Takada, M. (1999). Corticostriatal and corticosubthalamic input zones from the presupplementary motor area in the macaque monkey: Comparison with the input zones from the supplementary motor area. *Brain Research*, *833*, 191–201.

Isoda, M., & Hikosaka, O. (2007). Switching from automatic to controlled action by monkey medial frontal cortex. *Nature Neuroscience*, *10*, 240–248.

Jansons, K. M., & Alexander, D. C. (2003). Persistent angular structure: New insights from diffusion MRI data. *Information Processing in Medical Imaging*, *18*, 672–683. Dummy version.

Jernigan, T. L., Gamst, A. C., Fennema-Notestine, C., & Ostergaard, A. L. (2003). More "mapping" in brain mapping: Statistical comparison of effects. *Human Brain Mapping*, *19*, 90–95.

Jernigan, T. L., Trauner, D. A., Hesselink, J. R., & Tallal, P. A. (1991). Maturation of human cerebrum observed in vivo during adolescence. *Brain*, *114*(Pt 5), 2037–2049.

Johansen-Berg, H., Behrens, T. E., Robson, M. D., Drobnjak, I., Rushworth, M. F., Brady, J. M., et al. (2004). Changes in connectivity profiles define functionally distinct regions in human medial frontal cortex. *Proceedings of the National Academy of Sciences United States of America*, *101*, 13335–13340.

Lebel, C., Walker, L., Leemans, A., Phillips, L., & Beaulieu, C. (2008). Microstructural maturation of the human brain from childhood to adulthood. *Neuroimage*, *40*, 1044–1055.

Liston, C., Watts, R., Tottenham, N., Davidson, M. C., Niogi, S., Ulug, A. M., et al. (2006). Frontostriatal microstructure modulates efficient recruitment of cognitive control. *Cerebral Cortex*, *16*, 553–560.

Logan, G. D., & Cowan, W. B. (1984). On the ability to inhibit thought and action: A theory of an act of control. *Psychological Review*, *91*, 295–327.

Madler, B., Drabycz, S. A., Kolind, S. H., Whittall, K. P., & MacKay, A. L. (2008). Is diffusion anisotropy an accurate monitor of myelination? Correlation of multicomponent T2 relaxation and diffusion tensor anisotropy in human brain. *Magnetic Resonance Imaging*, *26*, 874–888.

Nachev, P., Wydell, H., O'neill, K., Husain, M., & Kennard, C. (2007). The role of the pre-supplementary motor area in the control of action. *Neuroimage*, *36*(Suppl. 2), T155–T163.

Nichols, T. E., & Holmes, A. P. (2002). Nonparametric permutation tests for functional neuroimaging: A primer with examples. *Human Brain Mapping*, *15*, 1–25.

Paus, T., Collins, D. L., Evans, A. C., Leonard, G., Pike, B., & Zijdenbos, A. (2001). Maturation of white matter in the human brain: A review of magnetic resonance studies. *Brain Research Bulletin*, *54*, 255–266.

Paus, T., Zijdenbos, A., Worsley, K., Collins, D. L., Blumenthal, J., Giedd, J. N., et al. (1999). Structural maturation of neural pathways in children and adolescents: In vivo study. *Science*, *283*, 1908–1911.

Pliszka, S. R., Glahn, D. C., Semrud-Clikeman, M., Franklin, C., Perez, R., III, Xiong, J., et al. (2006). Neuroimaging of inhibitory control areas in children with attention deficit hyperactivity disorder who were treatment naive or in long-term treatment. *American Journal of Psychiatry*, *163*, 1052–1060.

Reese, T. G., Heid, O., Weisskoff, R. M., & Wedeen, V. J. (2003). Reduction of eddy-current-induced distortion in diffusion MRI using a twice-refocused spin echo. *Magnetic Resonance in Medicine*, *49*, 177–182.

Rieger, M., Gauggel, S., & Burmeister, K. (2003). Inhibition of ongoing responses following frontal, nonfrontal, and basal ganglia lesions. *Neuropsychology*, *17*, 272–282.

Rubia, K., Smith, A. B., Brammer, M. J., & Taylor, E. (2003). Right inferior prefrontal cortex mediates response inhibition while mesial prefrontal cortex is responsible for error detection. *Neuroimage*, *20*, 351–358.

Rueckert, D., Sonoda, L. I., Hayes, C., Hill, D. L., Leach, M. O., & Hawkes, D. J. (1999). Nonrigid registration using free-form deformations: Application to breast MR images. *IEEE Transactions on Medical Imaging*, *18*, 712–721.

Schwartz, E. D., Cooper, E. T., Fan, Y., Jawad, A. F., Chin, C. L., Nissanov, J., et al. (2005). MRI diffusion coefficients in spinal cord correlate with axon morphometry. *Neuroreport*, *16*, 73–76.

Smith, S. M., Jenkinson, M., Johansen-Berg, H., Rueckert, D., Nichols, T. E., Mackay, C. E., et al. (2006). Tract-based spatial statistics: Voxelwise analysis of multi-subject diffusion data. *Neuroimage*, *31*, 1487–1505.

Smith, S. M., Jenkinson, M., Woolrich, M. W., Beckmann, C. F., Behrens, T. E., Johansen-Berg, H., et al. (2004). Advances in functional and structural MR image analysis and implementation as FSL. *Neuroimage*, *23*(Suppl. 1), S208–S219.

Snook, L., Paulson, L. A., Roy, D., Phillips, L., & Beaulieu, C. (2005). Diffusion tensor imaging of neurodevelopment in children and young adults. *Neuroimage*, *26*, 1164–1173.

Song, S. K., Sun, S. W., Ju, W. K., Lin, S. J., Cross, A. H., & Neufeld, A. H. (2003). Diffusion tensor imaging detects and differentiates axon and myelin degeneration in mouse optic nerve after retinal ischemia. *Neuroimage*, *20*, 1714–1722.

Song, S. K., Yoshino, J., Le, T. Q., Lin, S. J., Sun, S. W., Cross, A. H., et al. (2005). Demyelination increases radial diffusivity in corpus callosum of mouse brain. *Neuroimage*, *26*, 132–140.

Sowell, E. R., Thompson, P. M., Leonard, C. M., Welcome, S. E., Kan, E., & Toga, A. W. (2004). Longitudinal mapping of cortical thickness and brain growth in normal children. *Journal of Neuroscience*, *24*, 8223–8231.

Stuphorn, V., & Schall, J. D. (2006). Executive control of countermanding saccades by the supplementary eye field. *Nature Neuroscience*, *9*, 925–931.

Tomaiuolo, F., MacDonald, J. D., Caramanos, Z., Posner, G., Chiavaras, M., Evans, A. C., et al. (1999). Morphology, morphometry and probability mapping of the pars opercularis of the inferior frontal gyrus: An in vivo MRI analysis. *European Journal of Neuroscience*, *11*, 3033–3046.

van den Wildenberg, W. P., van Boxtel, G. J., van der Molen, M. W., Bosch, D. A., Speelman, J. D., & Brunia, C. H. (2006). Stimulation of the subthalamic region facilitates the selection and inhibition of motor responses in Parkinson's disease. *Journal of Cognitive Neuroscience*, *18*, 626–636.

Williams, B. R., Ponesse, J. S., Schachar, R. J., Logan, G. D., & Tannock, R. (1999). Development of inhibitory control across the life span. *Developmental Psychology*, *35*, 205–213.

Wolbers, T., Schoell, E. D., & Buchel, C. (2006). The predictive value of white matter organization in posterior parietal cortex for spatial visualization ability. *Neuroimage*, *32*, 1450–1455.